Metallurgical investigation of a plate from the bow visor from M/S Estonia

Technical Report

I.Westermann

Department of Materials Science and Engineering
Norwegian University of Science and Technology

The Plate

The received plate has been cut from the bottom side of the visor and is marked #4536. The plate is 600 mm long and the piece is curved and on the widest 230 mm wide, as shown in Figure 1. The total plate width, unfolded, is 490 mm on the widest. Figure 2 shows the bow visor and indicates where the plate has been removed from, note that the plate has been bend outwards according to how it is shown in Figure 1. The bow visor was raised on the 18th of November 1994, 52 days after the sinking[1]. It was according to the JAIC report first moved to Finland and later moved to Muskö Örlogsbas where it has been stored under roof. It is unsure when the plate was removed from the visor, but is expected to have occurred in relation to the official accident investigation. To the left in Figure 3, a butt weld is observed that runs perpendicular to the bend. The weld is fractured in the bend region. Some paint is left in some regions, where both red, blue and white is observed, but the majority of the plate is rusty. Some of the paint observed to the right in Figure 3 seem black and burned, but this, however, is expected to come from the cutting. The cut edge is further out on the backside of the bend plate in Figure 3. The upper side contains the fracture that has occurred in connection to the bending. The fracture line has a mixed mode of both clear edges and rough, thick and smooth surface fracture – in general very complex fracture. Two grooves are observed on top of the plate in the region where there is a general thickening of the plate (these are also observed in Figure 8). The plate was, in the less affected region (the cut out square in Figure 3), measured to be 10.6 mm thick. Focus in the investigation has been on the upper side of the plate, and in a region ~10 to 35 cm distance from the butt weld along the fracture line. Figure 4 shows the backside of the plate near the butt weld. None of the investigated samples are taken from an area influenced by this perpendicular weld. It is, however, unsure what the adjacent region parallel to the fracture line has been exposed to.

[1] Joint Accident Investigation Commission of Estonia, Finland and Sweden, JAIC report

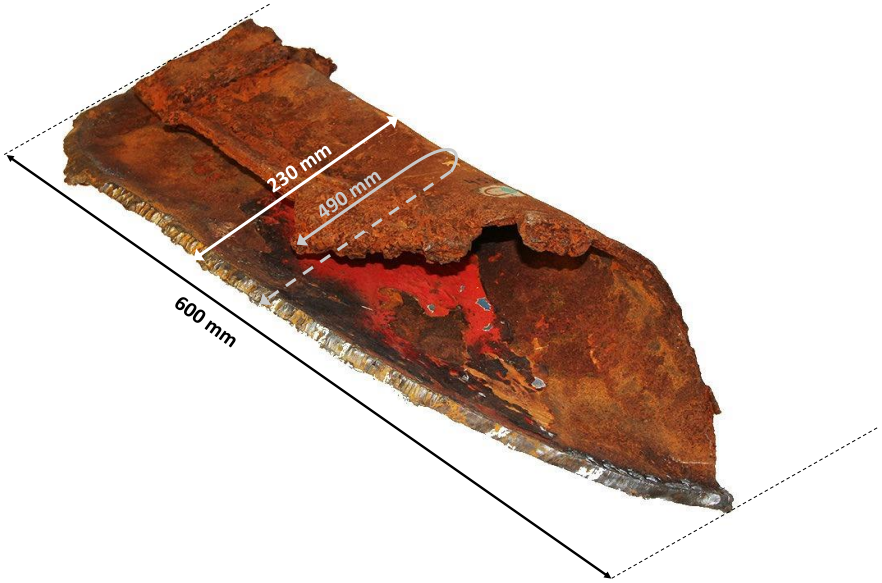

Figure 1 Measures of the plate of interest

Figure 2 Location of the plate on the bow visor

Figure 3 Central parts of the plate

Figure 4 Backside of the plate showing the butt weld and the weld region. Samples are not directly located in the vicinity of any welds.

Experimental techniques used

The rough cutting of the plate has been done using a band saw. Finer cuts have been done using a water cooled Discotom saw with a ceramic cut-off wheel, to keep the heat generation to a minimum. Samples were mounted in epoxy for easier handling. Metallographic preparation was

done by water cooled grinding down to mesh 2400 SiC paper followed by diamond polishing down to 1 µm. Washing and cleaning with ethanol was performed between each step. The samples were examined in light optical microscope both as polished and etched in a 2% nital solution. The latter to reveal the microstructure.

Vickers hardness measurements were performed, primarily using 1 kg weight and a dwell time of 15 seconds. Microhardness measurements using 25 g were made in the ferritic and pearlitic phases in the reference region. For two of the samples the hardness was measured across the thickness with only one measurement per location, whereas in more homogenous microstructures, the hardness is an average of at least 5 measurements.

Some samples have been examined in the scanning electron microscopy (SEM) using standard secondary electron imaging and energy dispersive X-ray spectroscopy (EDS) for element analysis.

For comparison and to study the hardenability of the steel, a small sample from the unaffected region was heat treated and quenched to give an idea of the obtainable microstructure and hardness. The sample was put in the hot furnace at 1200 °C, kept there for 10 minutes and quenched in 13 °C warm seawater.

Unaffected reference region

The sample in the unaffected region was cut from the sample shown in Figure 5 where the microstructure in the cross section at the tip of the arrow was investigated.

Figure 5 The sample from the unaffected region was taken from the cross section that the arrow points to.

The microstructure, shown in Figure 6 and 7, reveals a ferritic/pearlitic microstructure with a grain size of approximately 15 µm. Microhardness indentations in the ferrite and the pearlite show a hardness of HMV 178 and HMV 242, respectively. This is the microstructure that is expected for a mild steel.

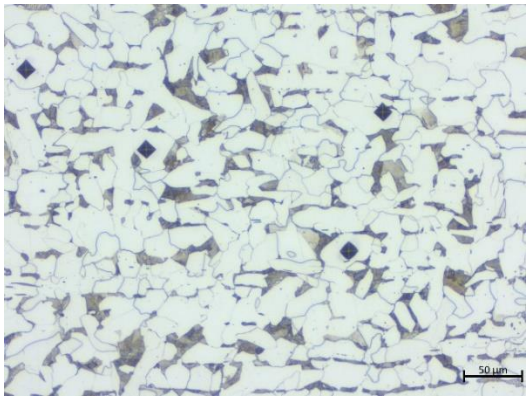

Figure 6 Ferritic/pearlitic microstructure. Microhardness indentations are seen in the ferritic grains.

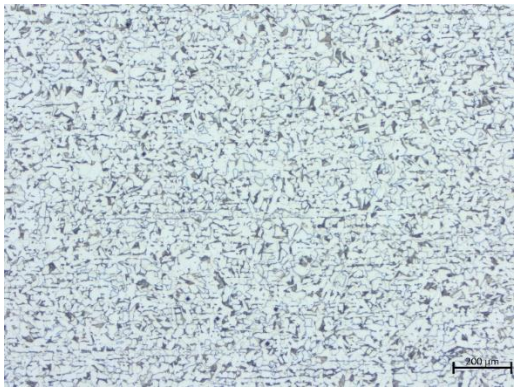

Figure 7 Lamellar ferritic/pearlitic structure at lower magnification than in Figure 6

Region adjacent to the reference area and near the fractured edge – sample 1

One sample was taken in the region next to the reference area towards the fracture line. Figure 8 shows the cross section of the plate where the sample has been taken. Also note the grooves observed at the top of the photo. This region shows a thinning of the plate approximately 6 cm from the fracture surface. The thickness in this region was measured to 5 mm. Parallel to the fracture line a thicker region is observed, comparable to a ridge of metal that has been pushed up from the thinner area. The total height of the ridge is measured to be in the magnitude of 15 mm. The fracture has occurred in a distance of approximately 30 mm from this ridge. A slightly thicker rust scale is observed from the thin region and towards the fracture line.

Figure 8 Cross section of the plate in the vicinity of the fracture line (to the right)

Figure 9 shows the cross section of the plate after metallographic preparation and etching. The fracture to the right shows necking and a ductile behavior. The ridge seems to be material that has been pushed up and metallographic bonded with a fine grained region in the middle and a region on both sides of this, where a surface area have been enclosed inside the material.

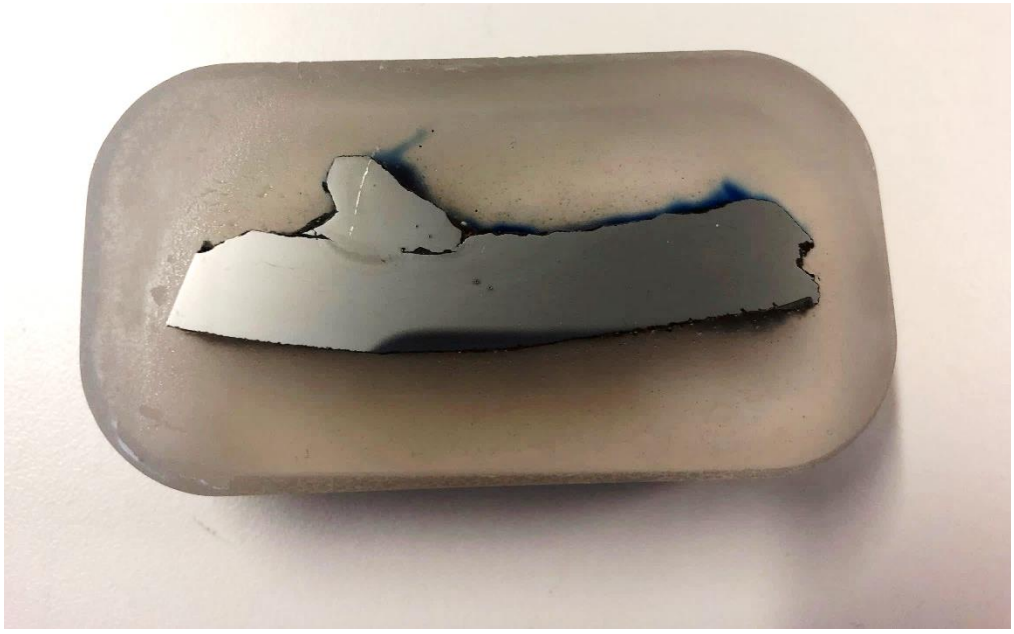

Figure 9 the metallographic prepared cross section of the sample.

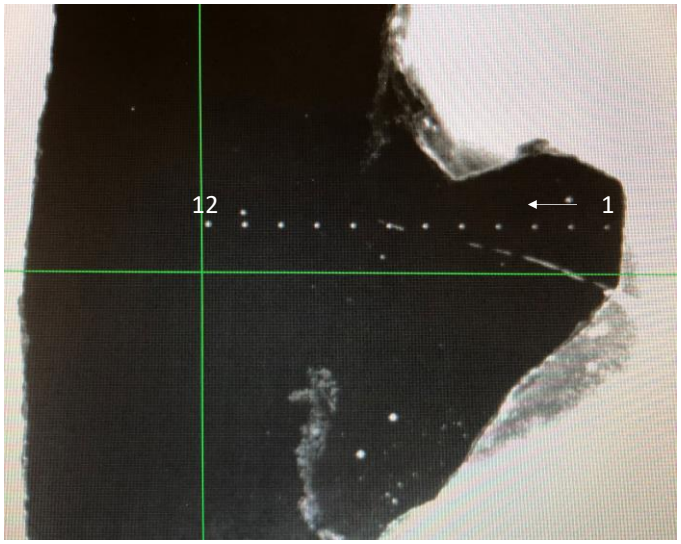

Figure 10 Hardness measurements were conducted in a line from right to left.

Table 1 Vickers hardness measurements along the line in Figure 10

test#	1	2	3	4	5	6	7	8	9	10	11	12
HV1	286	252	244	224	204	196	206	217	222	171	178	175

Vickers hardness measurements were conducted from the top of the ridge towards the center of the of the plate, see Figure 10 and Table 1. The hardness was found to be HV 286 at the top point of the ridge and descending through the ridge. A slight increase is seen in the fine grained region (points 7-9) and then decreasing again to the expected hardness of the plate. The first point (HV 286) at the outermost surface is assumed to be a martensitic structure.

The variation in microstructure across the interface is clearly visible in Figure 11, where the ferritic/pearlitic structure is visible in the bottom left corner, the pearlite becomes coarser and then a very fine grained structure is observed in the middle. In the upper right region a ferritic pearlitic region with ferrite along former austenitic grain boundaries, see Figure 12, is observed with a pearlitic interior. The former austenite grain size is in the order of 100 µm.

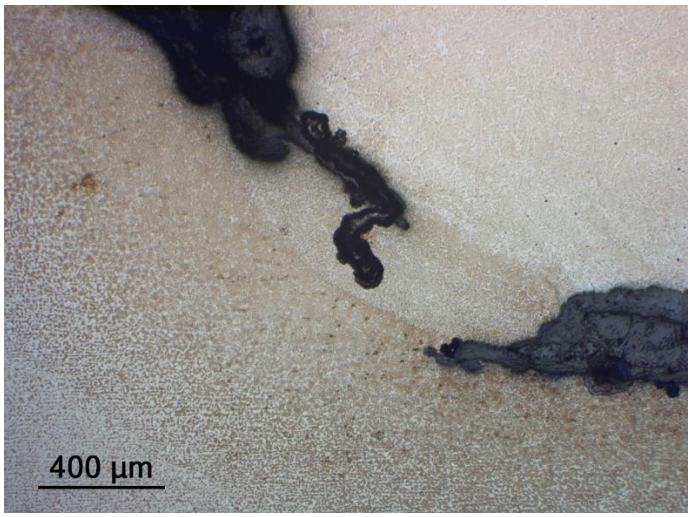

Figure 11 Joint region between the ridge cap and the base plate material.

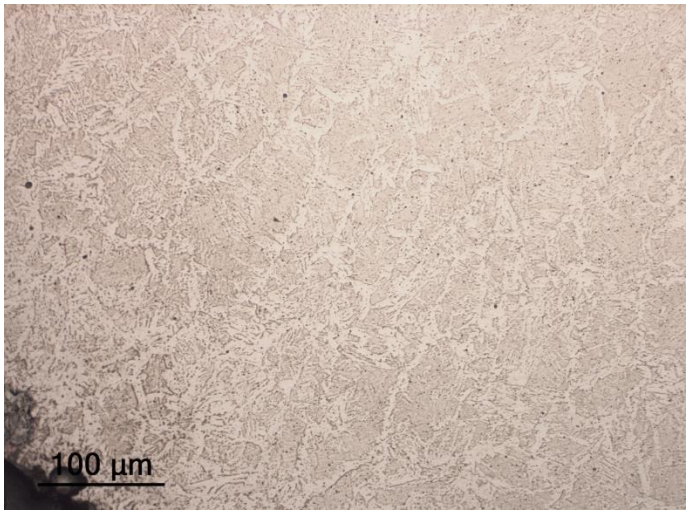

Figure 12 Microstructure in the ridge cap.

In the ridge cap a high amount of spherical black phases were observed as seen in Figure 13. There was a large variation in size, where the largest were in the size range of 50 µm in diameter. Figure 14 shows how the particles are randomly distributed in the microstructure.

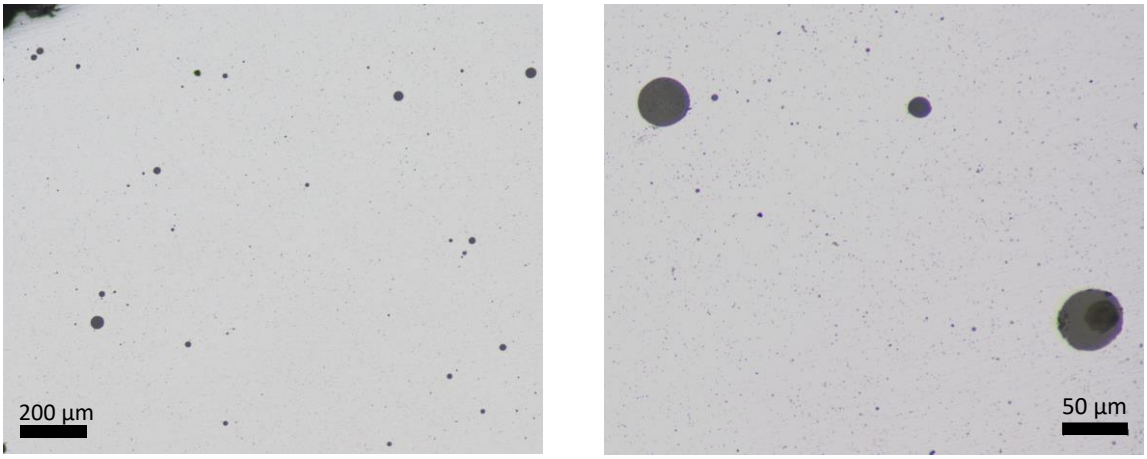

a) b)

Figure 13 Different magnifications of spherical phases in the ridge cap material.

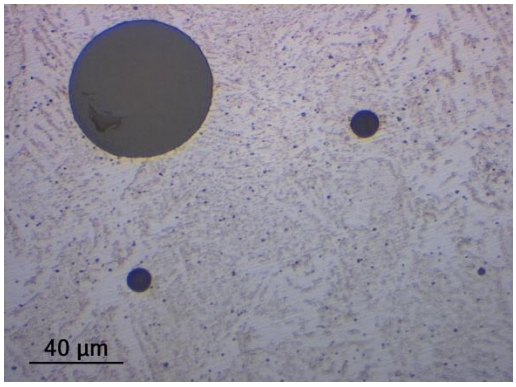

Figure 14 The black phases are randomly distributed in the etched microstructure and of various size.

EDS point analysis was conducted for two of the spherical particles, cf. Spectrum 8 and 9 in Figure 15. The results are shown in Figure 16 and 17.

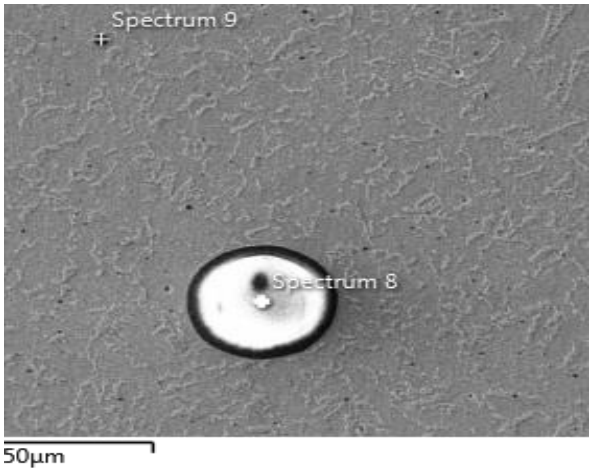

Figure 15 EDS point analysis was conducted for the two particles marked Spectrum 8 and Spectrum 9.

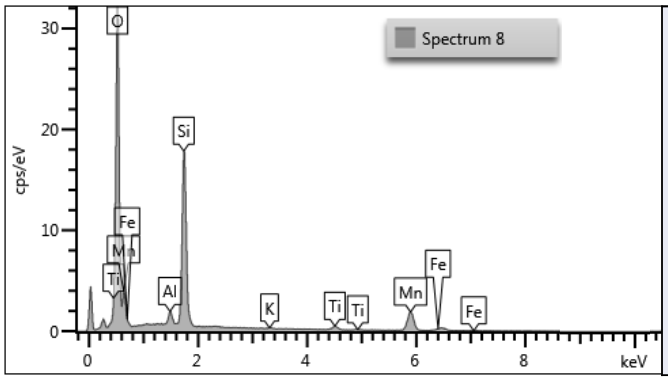

Element	Wt%
O	55,35
Al	1,69
Si	23,01
K	0,2
Ti	1,53
Mn	16,99
Fe	1,23
Total:	100

Figure 16 Element analysis of the large particle in Figure 15 (Spectrum 8)

Both the particles contain a large amount of Mn, Si and O. Spectrum 9 also indicates Fe, but since the particle is small, the surrounding matrix may contribute to the signal and should be considered a source of error. Small amounts of K and S are also detected. The K peak is very low, but the S peak in Figure 17 is significant. All elements are typical elements that can occur from production process of the steel. However, the Mn and Si levels are significantly high, and it is difficult to point to a specific source for such high levels of the elements. Mn and Si are often used as deoxidizer in welding filler wire, but from the macroscopic appearance of the plate with the thinning and the ridge it is difficult to see how the ridge would have been added as extra material. The thinning and ridge share similarities with features seen in explosion welding.

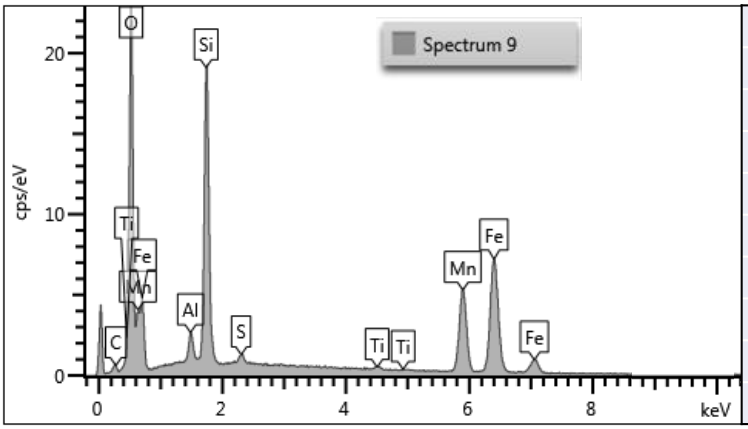

Element	Wt%
C	2,18
O	20,62
Al	1,42
Si	13,96
S	0,5
Ti	0,39
Mn	23,18
Fe	37,76
Total:	100

Figure 17 Element analysis of the smaller particle (Spectrum 9) in Figure 15

The investigation of the paint system from the bow visor lock[2] does not show any use of Mn in any of the paints used.

Figure 18 shows the light optical micrograph of the intermetallic regions between the ridge cap (top) and the base plate material (bottom). The intermetallic phase is porous and appears in different grey tones with some smaller white spots of steel phases. Attention should be drawn to the microstructure in the center region. A close up at higher magnification is shown in Figure 19.

[2] Research report RTE57243/96: Investigation of the paint systems from MV Estonia Visor Bottom Lock

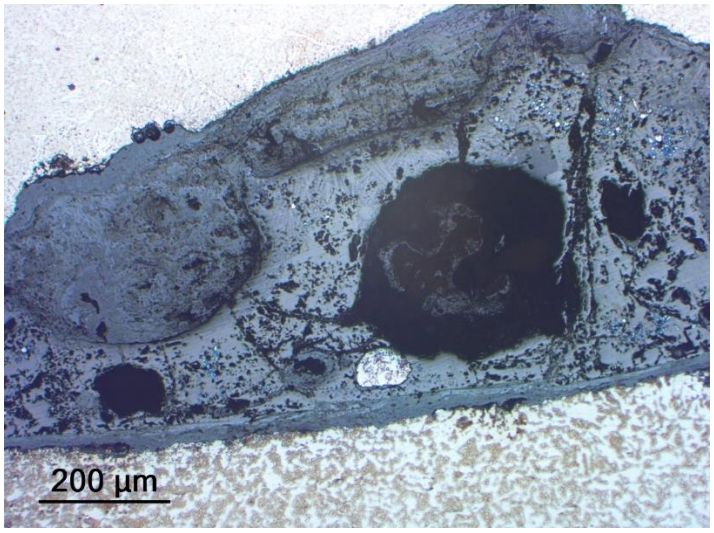

Figure 18 Light optical micrograph of the intermetallic region between ridge cap and base material

In Figure 19a, a dendritic microstructure is observed. This is a clear indication that the intermetallic phase has been in a liquid melted state and has solidified. Figure 19b shows the unetched microstructure from another place in the intermetallic region. Here, the bright spots show tendencies of dendritic growth, whereas the surrounding grey region shows a cellular directed growth, where the grains are of ~5 µm widths and in the range of 100 µm length. Indications of dendritic character are seen occasionally along the boundary. This indicates that the solidification rate of this grey phase has been so slow that cellular structure and not dendritic structure has formed.

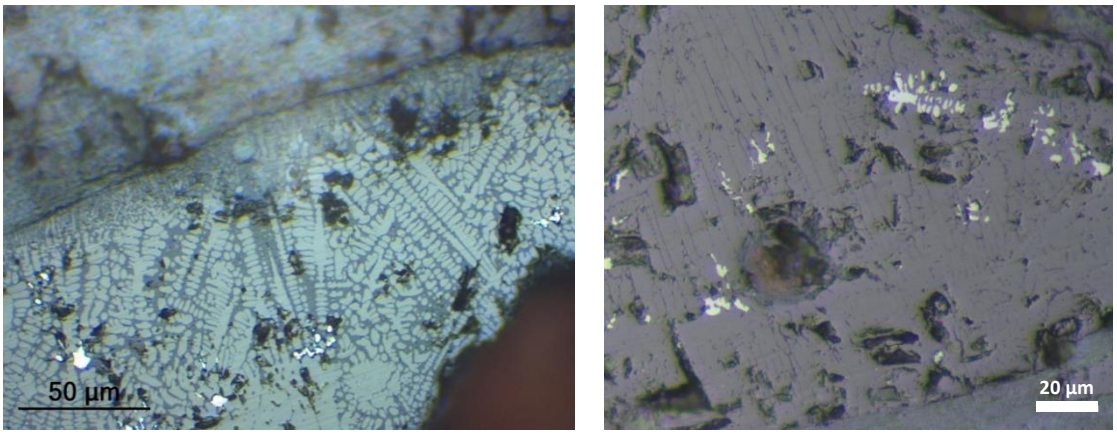

a) b)

Figure 19 a) Dendritic growth in the intermetallic phase, b) the unetched microstructure showing cellular growth in the intermetallic phase.

EDS analysis from the dendritic phase, e.g. spectrum 1 and 3 in Figure 20, reveals that the phase contains the amount of elements according the table listed in Figure 21. Fe, O, Mn and C are the main elements in this phase. O and C is usually difficult to quantify by EDS, but it is reasonable to believe that the elements are present within in the phase. It is reasonable to believe that this is melted iron oxide, and the temperature is estimated to be above 1200 °C.

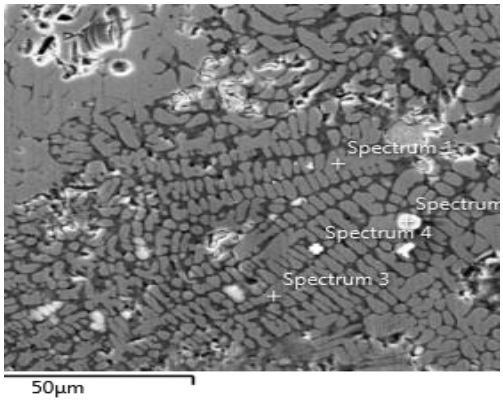

Figure 20 The region of interest where the EDS analysis was performed.

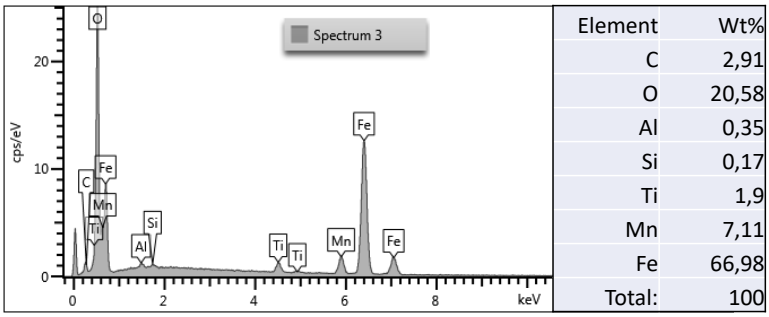

Element	Wt%
C	2,91
O	20,58
Al	0,35
Si	0,17
Ti	1,9
Mn	7,11
Fe	66,98
Total:	100

Figure 21 The EDS spectrum from the dendritic structure in Spectrum 3 in Figure 21.

The EDS spectrum from the eutectic region is shown in Figure 22. In addition to iron, oxygen and manganese, there is a higher level of Al and Si compared to the dendritic phase, as well as traces of S and K. Both S, K, Si, and Ti are elements that have been found in several of the paint systems, cf. reference 1, p. 9.

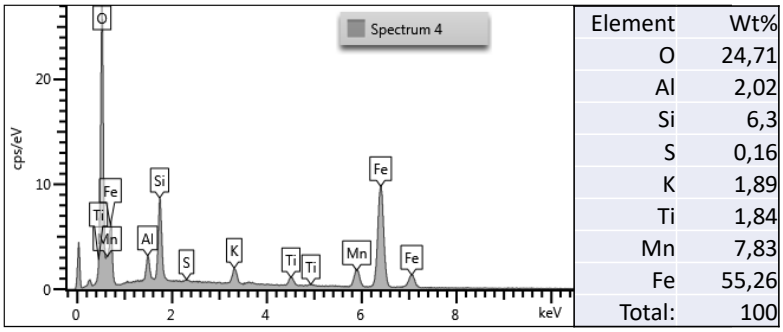

Element	Wt%
O	24,71
Al	2,02
Si	6,3
S	0,16
K	1,89
Ti	1,84
Mn	7,83
Fe	55,26
Total:	100

Figure 22 The EDS spectrum from the eutectic structure in Spectrum 4 in Figure 21.

Thick fracture area - sample 2

Two different samples were taken from the fracture area of the plate, where a clear thickening is observed. Figure 23 a) shows the piece that was cut from the plate, cf. Figure 3. The arrow indicates the cross section of interest shown in Figure 23 b). From Figure 23 a) it is seen that the fracture line in this region is complex with areas with a rough fracture and regions where the fracture is completely smooth.

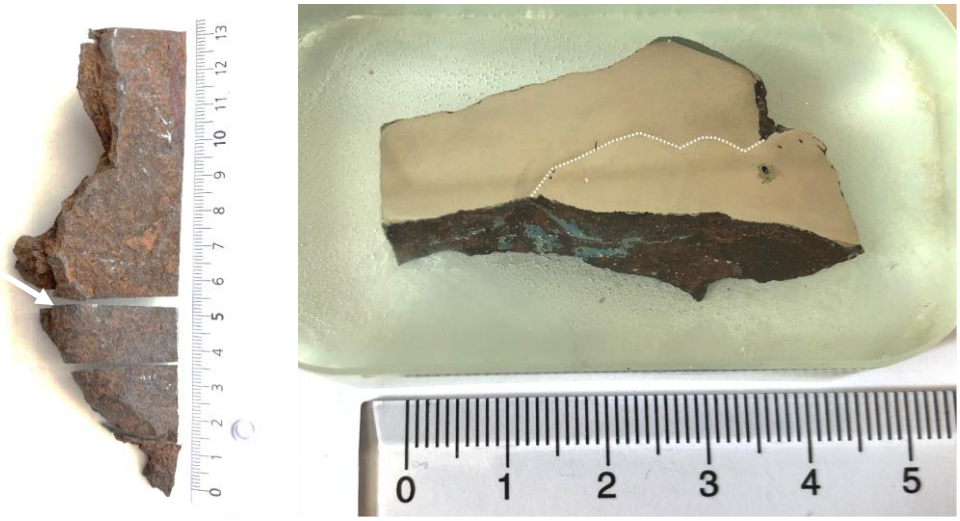

a b

Figure 23 The region with an increased thickness. A) the arrow indicates where the cross section shown in b) is taken from.

The area of interest in Figure 23 shows the etched surface. The white broken line indicates what could be a weld line. The primary reason for this assumption is that the blue paint on the back side seems to be continuous over the region. At maximum the sample here is 18 mm thick, and the length from the weld line to the tip of the fracture is 3 cm. The plate is at the top, above the weld line and the weld material underneath, this means the heat source has been from the other side compared to sample one. The fracture seems to be twofold, a vertical part above the broken line, and a 55° inclined ductile fracture at the lower part. The deformation direction of the microstructure at the fracture shows that the grains are elongated in a downwards direction, meaning that the plate must have been pushed up in the visor, opposite direction as the bend, from its original position. At the top of the sample there is a flat region, this can also be seen in Figure 23 a), where the microstructure shows a thin deformed layer, ~1 mm thick. Six larger pores are observed in this cross section, three in the vicinity to the weld line and three in the bulk material. Two of these are in the size range of 1 mm and were investigated in SEM and are shown Figure 24. The large pore in Figure 24 a) is 873 µm in maximum feret diameter and is seen as the large pore to the right in Figure 23 b). The elongated pore in Figure 24 b) is 970 µm long. In Figure 23 b) this is the vertical pore observed right above the dotted line to the left (it may also be seen in Figure 26 at the arrowhead). Nonconductive “threads” with a diameter 5-10 µm, Figure 25, were found inside these two pores. It is assumed that these are metal oxides. None of the other pores revealed similar findings. EDS results from these threads were difficult to interpret due to the charging of the region. The porosity in Figure 24 a) might be connected to the free surface enabling oxidation, but the elongated pore in Figure 24 b) is located in the very bulk material and it is, hence, unlikely that it extends to the surface.

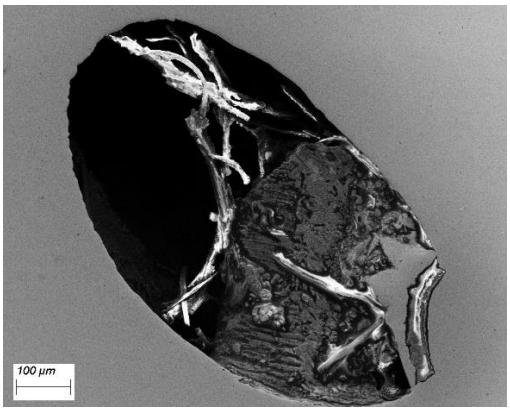

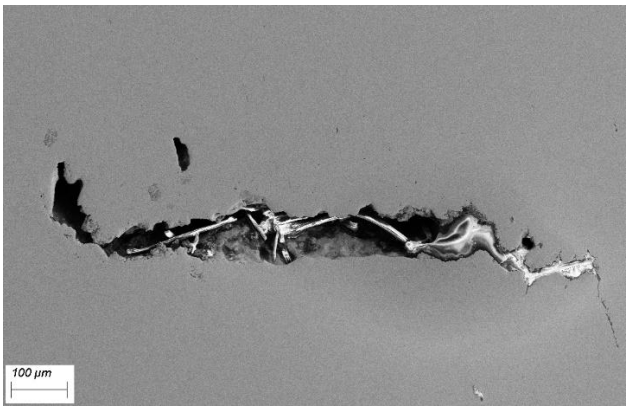

a) b)

Figure 24 Large porosities in sample 2 with metal oxide threads inside.

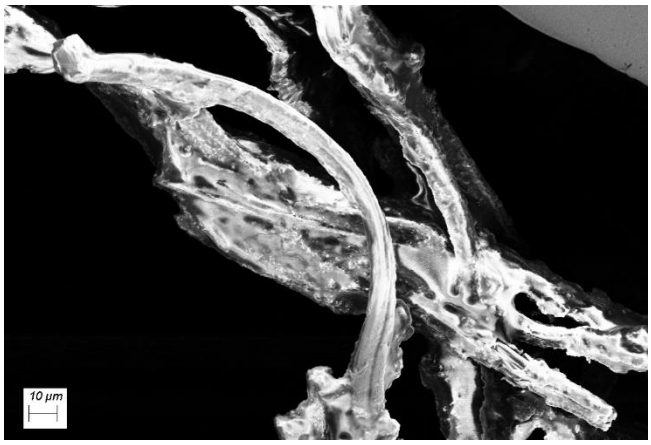

Figure 25 Close up of the metal oxides found in the pore in Figure 24 a).

Hardness measurements were conducted according to Figure 26 and are listed in Table 2. In the upper part (measurement 1-17) of the sample where a ferritic/pearlitic microstructure is found, the average hardness was found to be HV 164. When entering the lower region the hardness increased to HV 200.

Figure 26 Indication of the hardness measurements across the interface of sample 2.

Table 2 Hardness of the cross section of sample 2.

Test#	HV1	Test#	HV1	Test#	HV1	Test#	HV1
1	166	9	158	17	176	25	210
2	176	10	171	18	194	26	204
3	167	11	163	19	192	27	211
4	164	12	158	20	193	28	197
5	157	13	161	21	197	29	203
6	168	14	161	22	196	30	201
7	157	15	161	23	200	31	199
8	154	16	171	24	197	32	202

Smooth fracture surface – sample 3

Sample 3 is taken from a region of the fracture line where the fracture was almost completely smooth, as seen in Figure 27. In Figure 27 b) the sample has been slightly inclined to give an idea of the surface topography. The macroscopic appearance of the fracture surface is difficult to assign a brittle or ductile mode.

a) b)

Figure 27 Sample 3 is taken from a region where the fracture surface is almost smooth.

The microstructure in this sample is extremely complex. Figure 28 shows from where in the sample the microstructure is found, and Figure 29 shows the larger micrographs. Inside the sample there is a larger pore of 5 mm length that contains intermetallic phases, and it is reasonable to believe that the smeared-out microstructure and fracture appearance has occurred when the plate was bend.

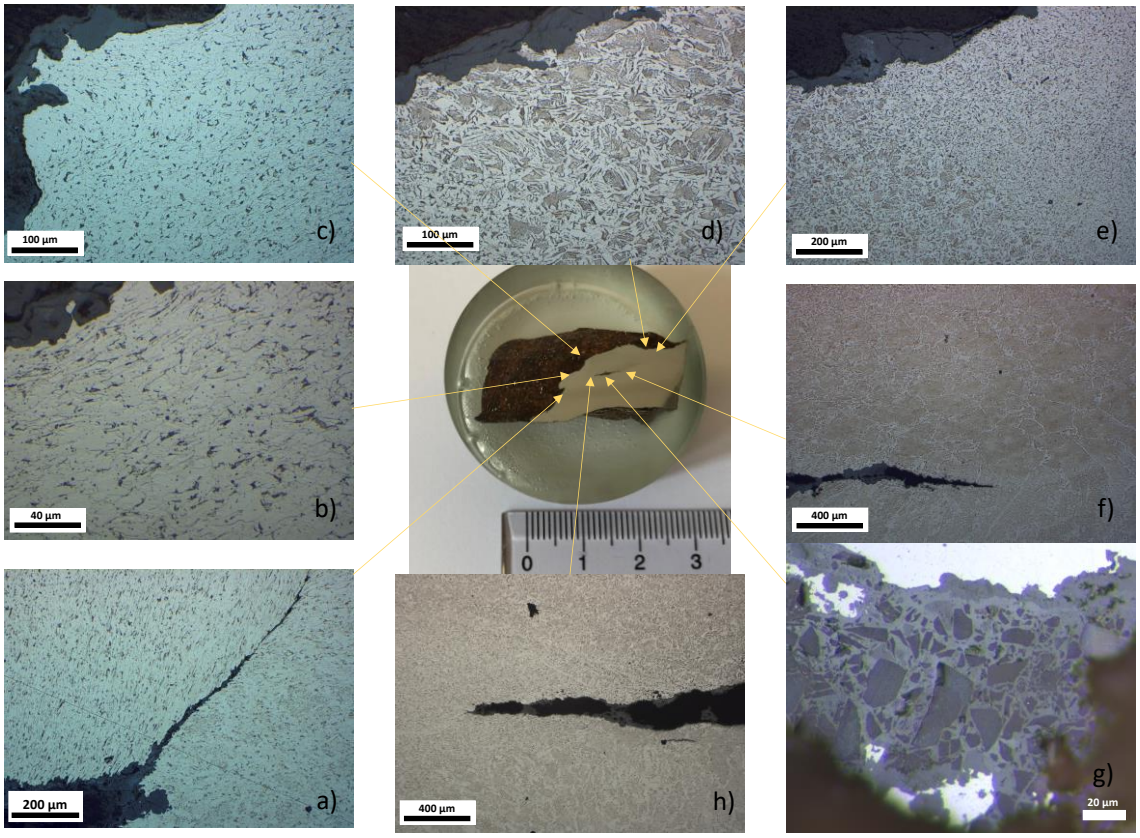

Figure 28 An overview of the regions where the different microstructures are found.

Figure 29 show larger micrographs of the different microstructures. In a) a crack is shown from the part of the fracture surface where it is believed that two different materials (two plates) have been smeared together. It is likely that the kissing surfaces seen in a) are the surfaces that extends to the

pore/crack in the interior. The microstructure consists of very fine-grained elongated ferrite ans spheroidized pearlite. Deformed ferrite is also observed in in b). The pearlite has been spheroidized into finely dispersed carbides. Spheroidization typically occurs in the temperature range 440°C - 750°C. This is in contrast to the more normal, but deformed, ferritic/pearlitic microstructure in c) where the size of the pearlitic grains is comparable to the reference material. Oxide/rust is observed along the fracture in Figures 29 a)-e). In figures d) and e) large variations from the normal structure is observed along the fracture surface. In d) a pearlitic structure with Widmanstätten ferrite is seen. This indicates that the microstructure has been heated above A_3 and cooled with a rather high cooling rate to obtain the Widmanstätten structure. The former austenite grain size is in the range 50-100 µm. In e) the rapid change in microstructure from coarse to finer grains along the fracture surface is observed. A coarse Widmannstätten grain structure is detrimental for the fracture toughness, but it is difficult to say when this transformation occurred, if it was prior to or in connection to the failure. The tips of the pore/crack are shown in f) and h). There is a difference in the adjacent microstructure from the crack tip closest to the fracture, h), or further away from the fracture, f). In f) a very fine lamellae pearlite with ferrite bands indicating former austenite grains. Some fine Widmanstätten ferrite is also observed. Noticeable is the size of the former austenite grains which are up to several hundred micrometers in length. Inside the pore/crack large regions with oxides and intermetallic phases were observed. In g) such a region is shown, where pointy and angular shaped dark grey intermetallic phases are observed in a lighter grey matrix. Some of the dark grey phases seems to have cracked in a brittle manner.

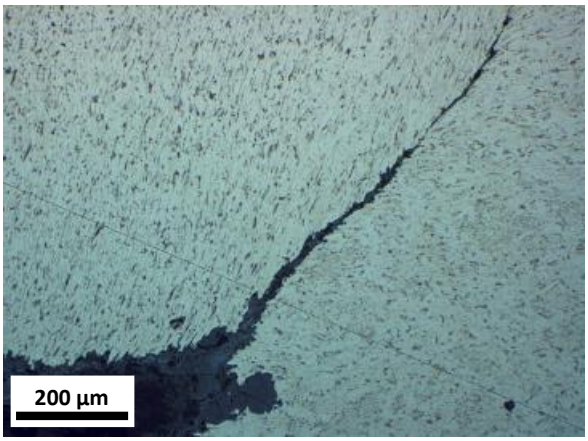

a)

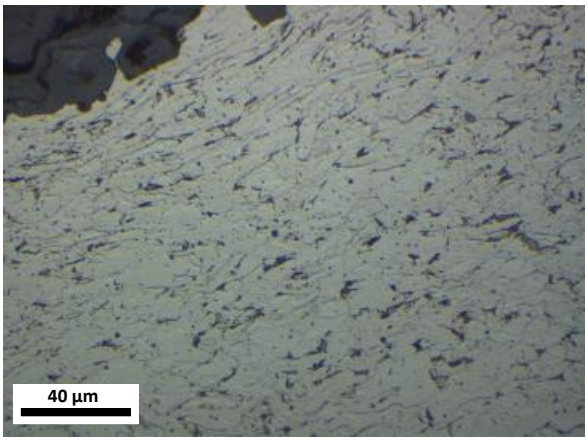

b)

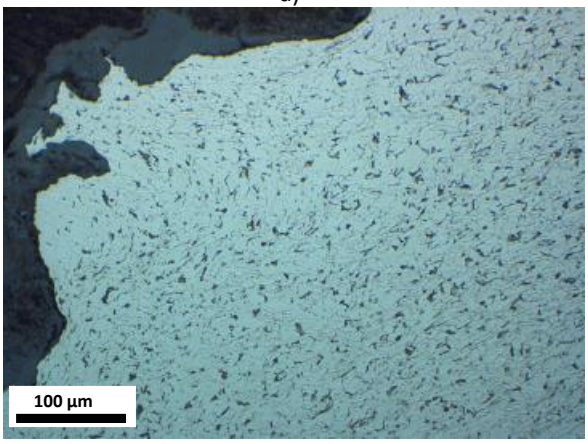

c)

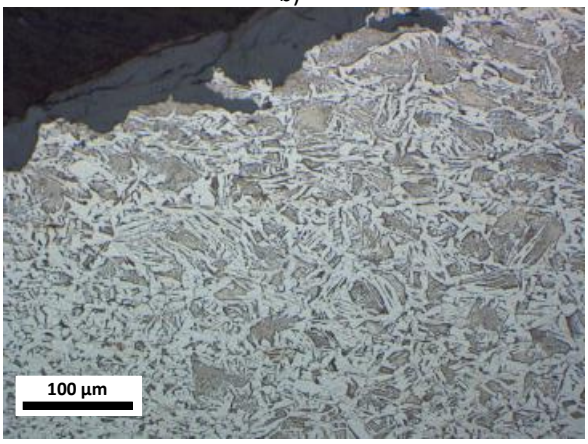

d)

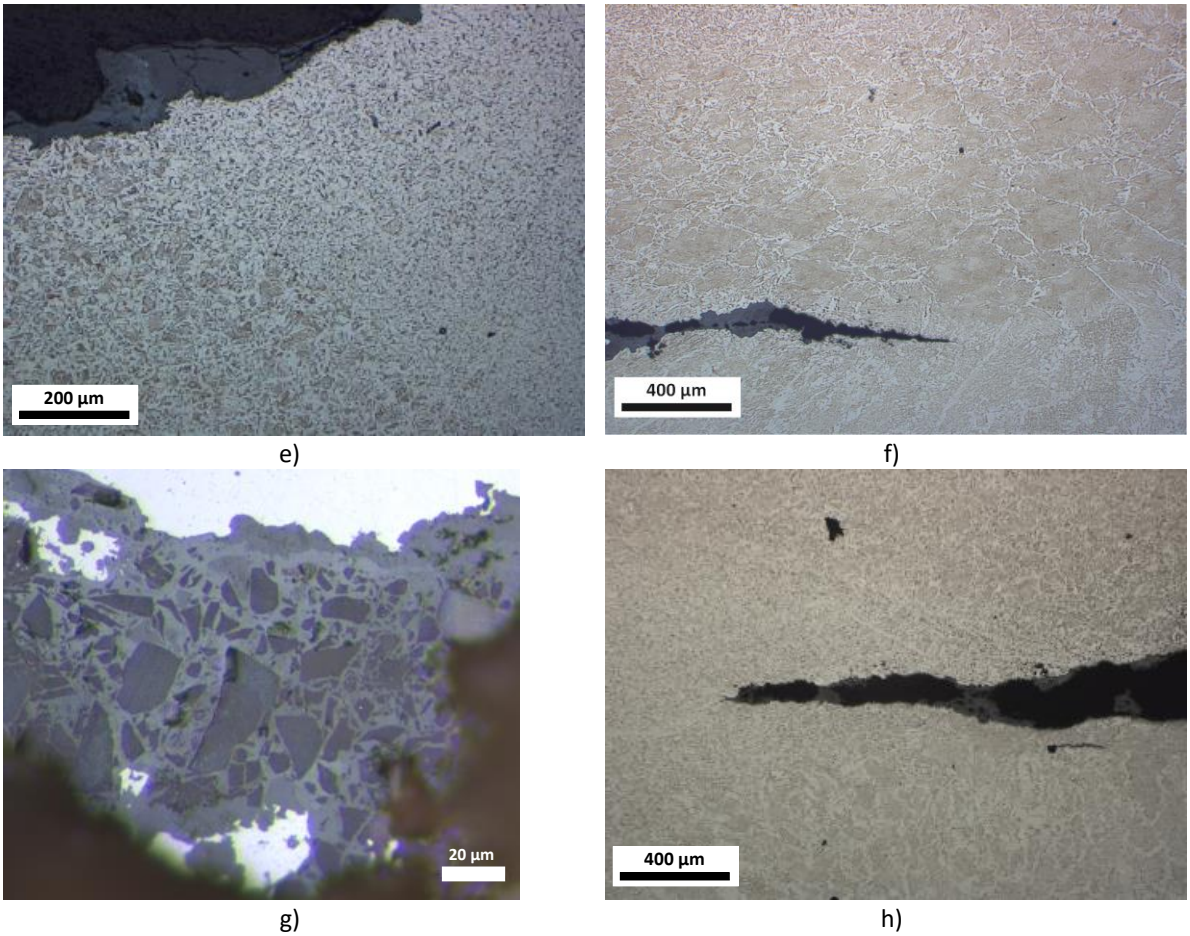

Figure 29 Larger micrographs of the microstructures in Figure 28.

The material underneath the pore/crack seems less affected than the upper part. But as seen from Figure 30, which is from the outermost pointy part of the fracture, the microstructure shows large and elongated grains where the cementite rich part is surrounded by ferrite and some Widmanstätten ferrite is also observed here.

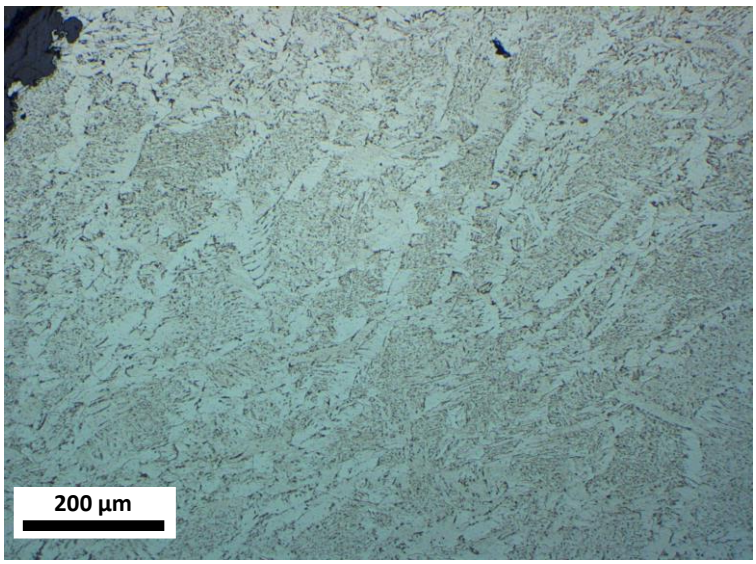

Figure 30 The microstructure in the pointiest part of the fracture

Quenching experiment

Mild steels are difficult to harden due to the low carbon content. To get an idea of the microstructure and obtainable hardness, a small sample was taken from the reference sample and put in a 1200 °C hot furnace. The sample was kept there for 10 minutes and then quenched in 13 °C cold sea water. The average hardness of 6 measurements was found to be HV1 295. The microstructure with a mixture of ferrite and martensitic needles is seen in Figure 31. None of the observed microstructures in the investigated plate is similar to the hardened microstructure.

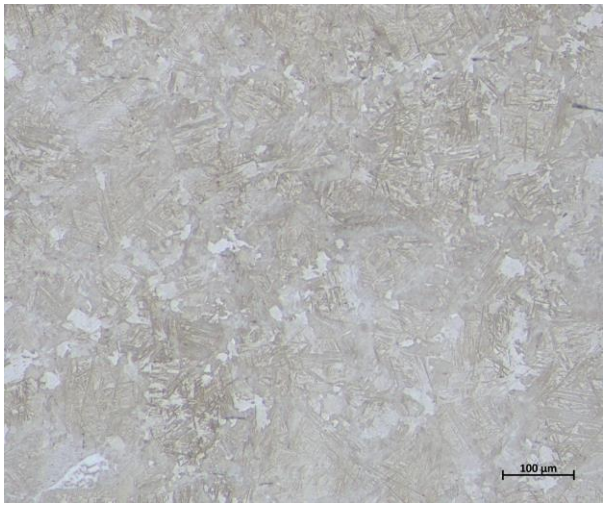

Figure 31 The microstructure of a hardened reference sample.

Summary

Several regions from the plate from the bow visor of M/S Estonia has been investigated. The plate was severely distorted and bend almost 180 degrees. Near the fracture line there are no obvious signs of any welds, but one of the investigated samples indicates that there might have been a weld in the vicinity or opposing side of the fracture. In this sample several pores were found. In the two largest ones (~1 mm in size), thread like intermetallics were found inside the pores.

Parallel to a part of the failure line a combined thinning and thickening (ridge) of the plate is observed. The microstructure in the ridge cap indicates that the microstructure has been heated to the austenite region. Spherical particles containing Mn, Si and O in the size range up to 50 µm were observed in the ridge cap. At the interface between the ridge cap and the base plate, regions with intermetallic phases with dendritic and cellular structures were found. This indicates the temperature locally has exceeded the melting point of the intermetallic phase. The heat source in this region is from the back side of the plate, opposite side as the possible weld mentioned above.

One of the samples has a very smooth fracture surface and it is difficult to tell whether it is a ductile or brittle fracture based on the appearance. The cross-section indicates both a ductile deformed ferritic/pearlitic microstructure along the fracture, but also a microstructure with large former austenite grains with ferrite (Widmanstätten) along the grain boundaries and pearlitic interior, which suggests a brittle structure. A 5 mm long pore/crack indicates that two materials have been deformed simultaneously. Intermetallic phases inside the pore/crack have fractured in a brittle manner. The microstructure in this sample is very complex and the temperature has been well above A_3 as some of the grains in the vicinity of the crack are up to 400 µm in length. Based on the investigation it is, however, not possible to say whether this has happened before or in connection to the failure. This sample has been exposed to heat from both sides.